ENVIRONMENTAL RESEARCH
LETTERS

LETTER • OPEN ACCESS

Regional temperature extremes and vulnerability under net zero CO_2 emissions

To cite this article: Liam J Cassidy *et al* 2024 *Environ. Res. Lett.* **19** 014051

View the article online for updates and enhancements.

You may also like

- Effects of processing conditions on porosity features of polyurea cross-linked silica aerogels synthesized by ambient pressure drying
Ming Li, Ting Wang and Jia Zhang

- Accelerating China's power sector decarbonization can save lives: integrating public health goals into power sector planning decisions
Qian Luo, Fernando Garcia-Menendez, Jiang Lin et al.

- Zero emission targets as long-term global goals for climate protection
Joeri Rogelj, Michiel Schaeffer, Malte Meinshausen et al.

This content was downloaded from IP address 1.146.92.231 on 16/05/2024 at 08:48

ENVIRONMENTAL RESEARCH
LETTERS

LETTER

Regional temperature extremes and vulnerability under net zero CO_2 emissions

Liam J Cassidy[1,2,*], **Andrew D King**[1,2], **Josephine R Brown**[1,2], **Andrew H MacDougall**[3], **Tilo Ziehn**[4], **Seung-Ki Min**[5] and **Chris D Jones**[6]

[1] School of Geography, Earth, and Atmospheric Sciences, University of Melbourne, Melbourne, Victoria, Australia
[2] ARC Centre of Excellence for Climate Extremes, University of Melbourne, Melbourne, Victoria, Australia
[3] Climate & Environment, St. Francis Xavier University, Antigonish, Nova Scotia B2G 2W5, Canada
[4] CSIRO Environment, Aspendale, Victoria, Australia
[5] Division of Environmental Science and Engineering, Pohang University of Science and Technology, Pohang, Republic of Korea
[6] Met Office Hadley Centre, Exeter EX1 3PB, United Kingdom
[*] Author to whom any correspondence should be addressed.

E-mail: lccass@student.unimelb.edu.au

Keywords: Paris Agreement, climate extremes, ZECMIP, net zero

Supplementary material for this article is available online

OPEN ACCESS

RECEIVED
26 April 2023

REVISED
7 November 2023

ACCEPTED FOR PUBLICATION
30 November 2023

PUBLISHED
18 December 2023

Original content from this work may be used under the terms of the Creative Commons Attribution 4.0 licence.

Any further distribution of this work must maintain attribution to the author(s) and the title of the work, journal citation and DOI.

Abstract

Signatories to the Paris Agreement have pledged to keep global warming to well below 2 °C above pre-industrial levels and preferably below 1.5 °C above pre-industrial levels. Beyond over-shooting Paris Agreement warming levels followed by net negative emissions, achieving a state of net zero carbon dioxide emissions is required to satisfy Paris Agreement warming goals. Research on climate changes under net zero CO_2 emissions is very limited to date with no comprehensive analysis of changes in extremes. In this study, we use results from Earth System Models in the zero emissions commitment model intercomparison project to understand regional mean-state climate change patterns during a 100 year period following carbon dioxide emissions cessation. We also perform an initial study of the evolution of hot and cold monthly temperature extremes after net zero CO_2 emissions, including an assessment of how the change in frequency of temperature extremes affects areas of different levels of socioeconomic development based on regional Human Development Index (HDI). The results show that most land regions experience a fast and continuous cooling response following emissions cessation, with large areas of significant model agreement. In contrast, the Southern Ocean continues warming over the century after emissions cessation. The frequency of land-based local monthly high temperature extremes generally stays constant or decreases during the century after emissions cessation, however, decreases in heat extreme frequencies are generally less for locations with lower modern HDI than areas with higher HDI which suggests that inequality of climate change will remain an issue even after net zero CO_2 emissions. There is an evident emergence of local monthly cold extremes following emissions cessation with most significant impact over high HDI mid- and high-latitude land regions.

1. Introduction

The Intergovernmental Panel on Climate Change has assessed the current state of the global climate concluding that human-caused climate change has caused warming on land, within the ocean, and in Earth's atmosphere, with a likely global mean surface temperature increase from 1850–1900–2010–2019 of 0.8 °C–1.3 °C attributed to human influence (IPCC 2021). Anthropogenic climate change also has a proven impact on weather and climate extreme events, with virtual certainty that both frequency and intensity of heat extremes have increased since the mid-twentieth century because of human-caused climate change (IPCC 2021). In response to the observed effects of climate change, the Paris Agreement was agreed to in 2015 with the core goal of limiting the increase in global-average temperature to well below 2 °C above pre-industrial levels and pursuing efforts to limit the temperature increase to

© 2023 The Author(s). Published by IOP Publishing Ltd

1.5 °C above pre-industrial levels. From a geophysical science perspective, there is a requirement to reach at least net-zero CO_2 to limit human-induced global warming, along with reductions of other greenhouse gases (IPCC 2021). In a state of net zero CO_2 emissions, residual anthropogenic CO_2 emissions are balanced by anthropogenic negative emissions.

There have been several studies that have investigated climate response to reaching a state of net zero using state-of-the-art climate model simulations (Matthews and Caldeira 2008, Plattner *et al* 2008, Frölicher and Joos 2010, Gillett *et al* 2011, Zickfeld *et al* 2013, MacDougall *et al* 2020, Jenkins *et al* 2022). The most relevant studies to this research use the Zero Emissions Commitment Model Intercomparison Project (ZECMIP), which includes a collection of Earth System Models (ESMs) and ESMs of Intermediate Complexity (EMICs) configured in emissions-driven mode, where the carbon dioxide atmospheric concentration and downstream climate impacts are determined based on the model representations of the carbon cycle, as opposed to concentration-driven modeling where the atmospheric carbon dioxide concentration is prescribed. More information regarding the emissions driven configuration used in ZECMIP experiments can be found in Jones *et al* (2016).

MacDougall *et al* (2020), used the collection of ESMs and EMICs in ZECMIP (Jones *et al* 2019) to simulate heat and carbon redistribution and committed global warming following emission cessation. The simulations are initially run using a 1% per annum increase in CO_2 concentrations until specific diagnosed cumulative emissions are reached (750 PgC, 1000 PgC, and 2000 PgC), at which point emissions are set to zero and models freely evolve in an emissions-driven configuration; the initial 1% CO_2 per annum can be in either concentration-driven or emissions-driven mode depending on modeling agencies ability to avoid introducing shock to the model system when changing to the zero emissions phase of the experiment (Jones *et al* 2019). The ZEC, which is defined as the change in global mean surface temperature following a complete cessation of carbon dioxide emissions, has become a well-used metric. Researchers have analyzed ZEC on various timescales, but ZEC is now commonly analyzed over multi-decadal timescales which are more relevant for policymakers. MacDougall *et al* (2020) found that, following carbon dioxide emissions cessation, there was a rapid reduction in atmospheric CO_2 concentrations followed by a decreasing rate of decline, consistent with several other studies (Frölicher and Joos 2010, Gillett *et al* 2011). Additionally, MacDougall *et al* (2020) found that ZEC is most likely near zero on multi-decadal timescales, which is consistent with previous model experiments using EMICs (Plattner *et al* 2008) and emission driven ESMs of full complexity (Lowe *et al* 2009, Frölicher and Joos 2010, Gillett *et al* 2011).

In a more recent study MacDougall *et al* (2022) investigate multi-decadal regional scale committed warming patterns following CO_2 emissions cessation. ZEC is computed on a regional basis to better understand regional temperature variation following a complete cessation of carbon dioxide emissions. The authors find significant differences regionally in both the sign and magnitude of ZEC. For nearly all ESMs included in the study, there is cooling over both land and ocean on average, with a warming lag period immediately after emissions cessation. For most ESMs, there is large scale cooling over land globally, and most models show cooling trends over ocean regions, however with some models disagreeing on warming/cooling signs in multiple oceanic regions throughout the domain; large differences in land-ocean response are consistent with previous modeling studies of various types of experimental designs (Joshi *et al* 2008, Rugenstein *et al* 2019, King *et al* 2020).

Overall, research has shown a carbon redistribution between land, ocean, and atmosphere following emissions cessation, resulting in falling atmospheric CO_2 concentration (e.g. MacDougall *et al* 2020). Overall rates of land and ocean uptake of atmospheric CO_2 are key components in determining global surface temperature response after CO_2 emissions cessation MacDougall *et al* (2020). Global committed warming is projected to be near zero, however regional warming commitments can be significant with large uncertainty between current available models. The committed climate changes have been shown to depend on the cumulative carbon emissions at the time of emissions cessation.

While previous studies have explored global responses to net zero emissions, limited work has focused on connecting global-scale climate change to regional climate. Further research regarding regional climate change following net zero CO_2 emissions is important because achieving a stable global mean temperature within Paris Agreement goals is not the same as achieving stable climate in individual regions; further research can help build an understanding of regional changes and nuances post net zero CO_2 emissions. In addition, although many studies have considered changes in climate extremes using scenarios that reach periods of net zero CO_2 emissions (such as SSP1-1.9 and SSP1-2.6), analysis of temperature extremes using idealized net zero climate model experiments like ZECMIP has not been conducted. In this study, we address existing research gaps by, first, identifying robust regional warming and cooling patterns following a complete cessation of carbon dioxide emissions. Second, we present an analysis of how

the frequency of regional hot and cold monthly temperature extremes change following emissions cessation in the ZECMIP ensemble. Third, we investigate how changes in temperature extremes following net zero impact regions of varying socioeconomic development quantified using the Human Development Index (HDI).

2. Data and methods

2.1. The ZECMIP

The ZECMIP, a sub-project of CMIP6 (Eyring *et al* 2016), was designed to quantify temperature change following a complete cessation of CO_2 emissions (i.e. the ZEC), and to investigate the geophysical drivers behind the climate response to CO_2 emissions cessation (Jones *et al* 2019). Note, ZEC can be evaluated from emissions cessation of only CO_2 (MacDougall *et al* 2020), non-CO_2 gases such as CH_4 or N_2O (Matthews and Zickfeld 2012), or all anthropogenic emissions (Hare and Meinshausen 2006). However, on decadal timescales, ZEC from ceasing emission of all forcing agents tends to converge to ZEC values from cessation of only CO_2 emissions which makes ZECMIP a reasonable choice given the simulation lengths of participating ESMs.

In this work, ZECMIP experiment esm-1pct-brch-1000 PgC (called experiment A1 from hereon) was used, which corresponds to about 2 °C CO_2-induced warming relative to pre-industrial (Jones *et al* 2019). Experiment A1 sets CO_2 emissions to zero once cumulative CO_2 emissions reach 1000 PgC, after which models are allowed to freely evolve for at least 100 years. Table S1 shows the ESMs included in the analysis with expanded model descriptions available in Table A1 of MacDougall *et al* (2020); note, GFDL-ESM2M was the original submission to ZECMIP but has since been replaced by results from GFDL-ESM4. The models included in this analysis are the nine that were available on the Earth System Grid Federation Australian node as of January 2022.

2.2. Global and regional ZEC

ZEC is defined as the change in global temperature projected to occur following a complete cessation of CO_2 emissions (Matthews and Weaver 2010, MacDougall *et al* 2020). In this report, ZEC is quantified over multi-decadal intervals on a global average and an individual grid level (latitude–longitude) basis. Figure 1 shows a simple schematic which illustrates how ZEC is quantified using data from the MIROC-ES2L model as an example. In figure 1, the *1pctCO2* portion of the experiment is represented by the blue curve, which is initialized at the pre-industrial condition for each model. The red curve represents the temperature evolution following a complete cessation of carbon dioxide emissions, which occurs at time t_{NZ} in figure 1. The near-surface air temperature (tas) variable is used.

The CMIP variable for near surface air temperature (tas) is used for all temperature calculations. For each model in the ensemble, the baseline net zero climatology, $\overline{\text{tas}}_{NZ}$ from figure 1, is computed using a 20 year window centered at the time of branching denoted t_{NZ}; the 20 year baseline climatology is computed as the mean climate bounded by upper and lower bounds illustrated by the blue shaded time frame along the *1pctCO2* curve in figure 1. Once the baseline climatology is known, global ZEC time series are then computed for each model using equation (1):

$$\text{ZEC}(t) = \overline{\text{tas}}(t) - \overline{\text{tas}}_{NZ} \quad (1)$$

where $\text{ZEC}(t)$ is the time series representing the difference in global mean surface temperature evaluated at time t and the baseline climatology $\overline{\text{tas}}_{NZ}$. Figures S1 and S2 in the supplementary information show the global mean surface temperature anomalies and global ZEC time series for the nine ESMs, respectively. Comparable ZEC time series can be found in MacDougall *et al* (2020) figure 2(b).

To compute regional changes in ZEC, 20 year climatologies are computed for three unique time periods following emissions cessation. In this research, 20 year climatologies are centered at 25, 50, and 90 years after emissions cessation, consistent with previous research (MacDougall *et al* 2020, 2022). The three ZEC time frames are centered about t_{25}, t_{50}, and t_{90}, respectively as shown in figure 1; the three ZEC time frames are illustrated by the red shaded portions of the net zero CO_2 portion (red curve) shown in figure 1. Regional (lat, lon) distributions of ZEC for each ZEC time window (ZEC_{25}, ZEC_{50}, ZEC_{90}) are then computed using equation (2):

$$\text{ZEC}_Y(\text{lat,lon}) = \overline{\text{tas}}_Y(\text{lat,lon}) - \overline{\text{tas}}_{NZ}(\text{lat,lon}) \quad (2)$$

where $\overline{\text{tas}}_Y(\text{lat,lon})$ is the near-surface air temperature at each grid point (lat, lon) averaged over a 20 year window centered at the year defined by subscript Y (subscripted years include 25, 50, and 90). $\overline{\text{tas}}_{NZ}(\text{lat,lon})$ is the baseline climatology defined as an averaged 20 year window centered at the time associated with the net zero branch, t_{NZ}. Figure S3 shows baseline climatologies for each of the nine participating ESMs. Equation (2) is applied for each model within the ensemble ($n = 9$). Figures S4–S6 show the spatial distribution of ZEC_{25}, ZEC_{50}, and ZEC_{90} for the nine models included in the ensemble, respectively. As highlighted in MacDougall *et al* (2022), there are significant differences in regional projections of ZEC especially in high-latitudes. The significant differences in regional ZEC projections are noteworthy when considering ensemble mean results, especially

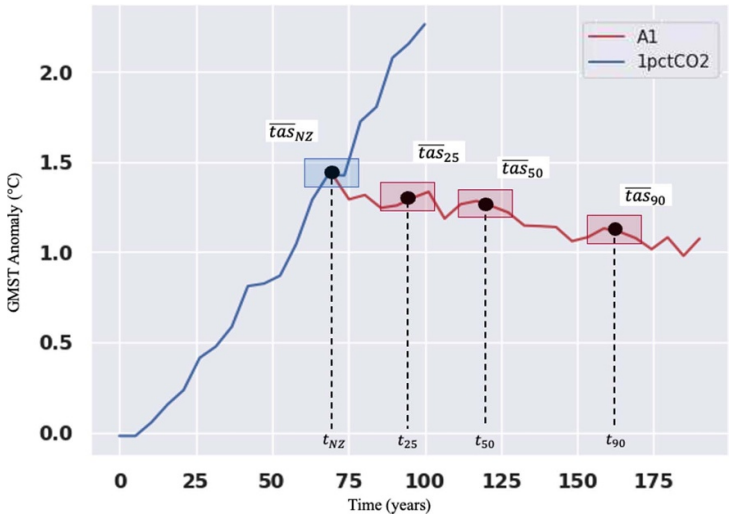

Figure 1. Illustration of baseline and ZEC climatologies (centered about years 25, 50, and 90 after emissions cessation) used to compute global and regional ZEC values. The red shaded boxes illustrate the 20 year time frames used for the ZEC climatologies and the blue shaded box illustrates the 20 year time frame used for the baseline net zero climatology. Note, the baseline net zero climatology uses only data from the *1pctCO2* curve.

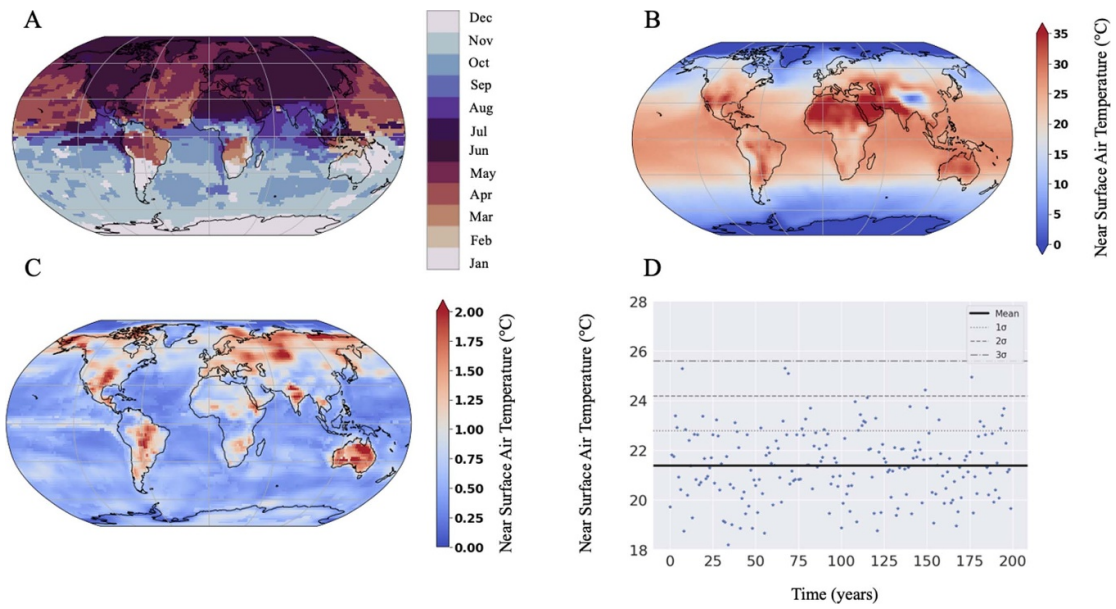

Figure 2. Using MIROC-ES2L pre-industrial control, (A) distribution of months associated with maximum local near surface air temperatures. (B) Mean near surface air temperature distribution from pre-industrial control associated with local maximum month. (C) Standard deviation distribution of near surface air temperatures from pre-industrial control associated with local maximum month. (D) Pre-industrial control mean near-surface air temperature and computed extreme levels 1–3σ for grid cell over Melbourne, Australia.

in areas such as Arctic latitudes where the largest spread between the models in the ensemble exists.

2.3. Local monthly temperature extremes

We assess how high temperature extreme events will evolve after net zero carbon dioxide emissions are achieved by investigating how temperatures during location-specific hottest months change after CO_2 emissions cessation. Local monthly hot temperature extreme thresholds are calculated using the means and standard deviations of the local monthly maximum temperature determined from the pre-industrial control simulation. Monthly temperature data was used so that all nine models could be included in the analysis. Similar methods have been used to study the historical precedence of the 2021 Pacific Northwest heatwave (Neal *et al* 2022). To compute extreme thresholds for local monthly maximum temperature extremes, first, the calendar month associated with local maximum monthly temperature was determined for each model using the pre-industrial control runs. Figure 2(A) shows a map with the distribution of months associated with maximum near surface air temperature using

the MIROC-ES2L model as an example. Maps of the month associated with maximum temperature were also created for the other models and can be found in figure S7.

After determining the month associated with monthly maximum temperature for each grid cell, ensemble means and standard deviations (σ) are computed for each grid cell's month of maximum temperature. Distributions of mean and standard deviation of local monthly maximum temperature from the *piControl* simulation are shown in figures 2(B) and (C), respectively. Peak mean temperatures are primarily located over tropical and mid latitude land surfaces. Standard deviation, which is indicative of natural variability in the unforced pre-industrial control experiment, is largest over land surfaces, with generally lower variability in the tropical latitudes. Thresholds of local monthly temperature extrema are then computed for each standard deviation level (σ-level) using equation (3):

$$\mathrm{tas}_{N\sigma}(\mathrm{mon}_{\max}, \mathrm{lat}, \mathrm{lon}) = \overline{\mathrm{tas}}(\mathrm{mon}_{\max}, \mathrm{lat}, \mathrm{lon}) + N * \sigma_{\mathrm{tas}}(\mathrm{mon}_{\max}, \mathrm{lat}, \mathrm{lon}) \quad (3)$$

where $\mathrm{tas}_{N\sigma}$ represents monthly extreme temperature distribution at a given σ-level,$\overline{\mathrm{tas}}$ represents the local (lat, lon) mean near surface air temperature for the month of maximum temperature, and σ_{tas} is the standard deviation of local (lat, lon) monthly maximum temperature. In the standard deviation term (second term, right hand side), the multiplier N is used to compute specific σ-level extreme thresholds. For this research, 1σ through 3σ extreme thresholds are considered for hot temperature extremes ($N = 1$, 2, or 3). As an example of a grid-based extreme temperature calculation, figure 2(D) depicts the mean and extreme thresholds 1σ–3σ for the closest grid cell over Melbourne, Australia (38° S, 144° E) using the MIROC-ES2L model. The data is specific to the pre-industrial control simulation restricted to the local month of maximum temperature (computed as February over Melbourne for the MIROC-ES2L ESM).

Frequencies of local (lat, lon) monthly hot temperature extreme exceedance are computed for the net zero baseline climatology (20 year window centered at the time of branching denoted t_{NZ} from figure 1), and for the ZEC_{25} and ZEC_{90} 20 year windows. The frequencies of monthly temperature extremes for the 20 year ZEC time frames and the 20 year baseline climatology express the percentage of years (out of 20) that a local grid cell exceeds local σ-level thresholds. Changes in frequency of local monthly hot temperature extremes are computed for the ZEC_{25} and ZEC_{90} 20 year time frames using equations (4) and (5):

$$\Delta f_{\mathrm{ZEC25}_{N\sigma}}(\mathrm{lat}, \mathrm{lon}) = f_{\mathrm{ZEC25}_{N\sigma}}(\mathrm{lat}, \mathrm{lon}) - f_{NZ_{N\sigma}}(\mathrm{lat}, \mathrm{lon}) \quad (4)$$

$$\Delta f_{\mathrm{ZEC90}_{N\sigma}}(\mathrm{lat}, \mathrm{lon}) = f_{\mathrm{ZEC90}_{N\sigma}}(\mathrm{lat}, \mathrm{lon}) - f_{NZ_{N\sigma}}(\mathrm{lat}, \mathrm{lon}) \quad (5)$$

where $f_{\mathrm{ZEC25}_{N\sigma}}$ and $f_{\mathrm{ZEC25}_{N\sigma}}$ are local (lat, lon) frequencies of σ-level ($N = 1$, 2, or 3) monthly temperature extremes for the ZEC_{25} and ZEC_{90} 20 year time windows, respectively. $f_{NZ_{N\sigma}}$ represents local (lat, lon) frequencies of σ-level ($N = 1$, 2, or 3) monthly temperature extremes for the 20 year net zero baseline climatology (centered at t_{NZ} from figure 1). Differences in extreme frequency over the century after emissions cessation are computed by subtracting the frequencies during the ZEC_{90} time window by frequencies during the ZEC_{25} time window.

Changes in local monthly cold extremes were also investigated. The methodology for defining cold extremes follows a similar approach as determining hot extremes, however for cold extremes, the σ-level thresholds are based on local minimum monthly temperatures determined for each grid cell. Additionally, extreme thresholds are computed using -0.25σ, -0.5σ, and -1σ for cold extremes because comparable thresholds to those used for the hot extremes analysis are rarely achieved after the simulated warming from the *1pctCO2* phase of the idealized experiment. Changes at these σ-levels are not always considered as extreme, however trends in -0.25σ, -0.5σ, and -1σ sigma level events will suggest changes in frequency of 'colder-than-average' cold months following net zero. Additionally, although the extreme level thresholds used for cold extremes here are less than thresholds used for heat extremes, cold extreme events at -1σ thresholds can cause damage and are still studied in current research (Dai *et al* 2021). For consistency with the local monthly hot extreme convention used in this research, we refer to changes in cold month frequencies as 'cold extremes' throughout the paper. The supplemental material includes an analysis and illustration that shows the method for computing local monthly cold extreme thresholds using a similar approach to the local monthly heat extreme analysis captured in figure 2. Figure S8 in the supplementary material shows the distribution of local coldest months for the nine ESMs. Using the MIROC-ES2L ESM as an illustrative example, figure S9 in the supplementary material shows distribution of months associated with minimum local near surface air temperatures, mean near surface air temperature distribution from pre-industrial control associated with local minimum month, standard deviation distribution of near surface air temperatures from pre-industrial control associated with local minimum month, and pre-industrial control mean near surface

air temperature and computed extreme levels—0.25σ through -1σ for grid cell over Melbourne, Australia.

2.4. Local monthly hot and cold extremes and the HDI

Less economically developed regions experience disproportionate loss and damage from climate extremes such as heatwaves, floods, and tropical storms (Gamble *et al* 2016, Birkmann *et al* 2022) To improve understanding of how the frequency of temperature extremes might affect populations with different levels of vulnerability following CO_2 emissions cessation, the relationship between local monthly maximum temperature extremes and local HDI was explored. HDI is a unique multidimensional measure of development and serves as an important alternative to some traditional single dimensional measures of development such as gross domestic product (Sagar and Najam 1998). HDI is a composite measure that considers length and health of life, access to education, and standard of living (Kummu *et al* 2018). HDI was chosen for this study as a measure of socioeconomic development because the HDI includes social indicators as well as economic development. Figure S10 shows the 2015 HDI distribution used in this study. HDI changes over time due to developments such as improvements in regional economic markets, increased access to healthcare, and advancements in local education. However, projections of HDI have not been developed in accordance with the CO_2 emissions cessation scenario used under the ZECMIP framework. Therefore, static regional HDI values based on the recent 2015 dataset from Kummu *et al* (2018) are used here. The HDI dataset from Kummu *et al* (2018) has been used in other studies examining inequality of climate change impacts (e.g. Lieber *et al* 2022).

3. Results

3.1. Regional ZEC

To provide a comprehensive projection of how ZEC varies spatially within the ensemble, median ZEC distributions for ZEC_{25} and ZEC_{90} time windows are shown in figures 3(A) and (B), respectively. The median was chosen here to avoid skewing regional results from the limited sample size ($n = 9$) towards outliers such as the CESM2 model which shows a strong inter-hemispheric temperature gradient after CO_2 emissions cessation. The inter-hemispheric relationship exhibited by CESM2 is shown in the supplemental material Figures S4–S6, and is also shown in figure 3 of MacDougall *et al* (2022). Additionally, to evaluate the change in ZEC over the century following carbon dioxide emissions cessation, the regional difference between median ZEC_{90} and ZEC_{25} was computed and is shown in figure 3(C). If at least eight of the nine ESMs show agreement in the sign of ZEC (or sign of change in ZEC in the case of figure 3(C)) then this corresponds to p-value <0.05 (calculated using the binomial distribution) and is taken to be statistically significant. Figure S13 in the supplemental material shows an illustration of the fundamental binomial distribution with a nine-model sample size. Although ESMs are not entirely independent (Knutti *et al* 2013), the ESMs participating in ZECMIP have a large diversity of component sub models as shown in tables A1 and A2 from MacDougall *et al* (2020).

The ZEC distributions show cooling or warming responses between -0.5 °C and 0.5 °C with significant regional variation consistent with previous work from MacDougall *et al* (2022). The global mean surface temperature decline 0.07 °C by the ZEC_{25} time frame and continues to decline an additional 0.14 °C over the century after CO_2 emissions cessation. An ensemble median global mean surface temperature drop of 0.16 °C over the century after CO_2 cessation is noteworthy considering the scale of global surface temperature goals established in the Paris Agreement (<2 °C above pre-industrial levels with efforts to limit to 1.5 °C). The model-specific global ZEC results are available in table S1 in the supplementary material. The regional ZEC distributions show a rapid cooling response over land with continued cooling as the ZEC time window reaches ZEC_{90}, with the largest land surface cooling occurring in the Northern Hemisphere. The largest warming is projected in the northeast Pacific Ocean, and Southern and Indian Ocean roughly between longitudes 70° W (Cape Horn, Chile) and 175° E (New Zealand). Overall, land exhibits greater cooling than the ocean likely because of differences in oceanic and land heat capacities, where land show quicker recovery to pre-industrial temperatures than ocean areas (MacDougall *et al* 2022). It is also possible that changes in local feedbacks and the hydrological cycle causes greater cooling over land than the ocean (Joshi *et al* 2008). There is an initial cooling by ZEC_{25} followed by a rebound in near-surface air temperature over the century after ZEC_{25} in the North Atlantic. This is possibly due to the evolution of Atlantic Meridional Overturning Circulation projected by the models; results from MacDougall *et al* (2022) suggest diverse evolution of AMOC between the models with some models showing an AMOC strengthening by the end of the century after CO_2 emissions cessation.

The ESMs show significant agreement of cooling over land, with increasing area of the planetary surface having significant model agreement by the ZEC_{90} time frame. There is also significant model agreement of cooling in tropical Atlantic, Indian, and western Pacific Oceans seen in the ZEC_{90} figure 3(B); this strong cooling agreement is driven by continued temperature changes between ZEC_{90} and ZEC_{25} as captured by the cross-hatching in figure 3(C). There is significant warming agreement within the ensemble

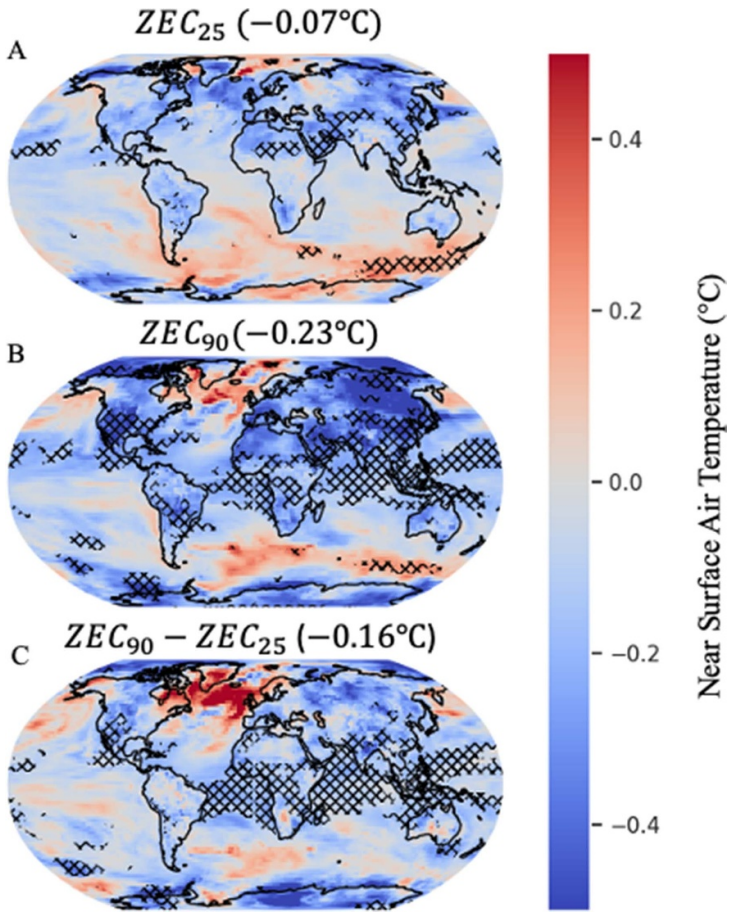

Figure 3. Ensemble median of (A) ZEC_{25} regional distribution and (B) ZEC_{90} regional distribution, and (C) difference between ZEC_{90} and ZEC_{25} distributions. In (A) and (B), cross-hatching indicates that at least 8 ESMs have the same sign of ZEC locally. In (C), cross-hatching indicates that at least 8 ESMs show same sign of change in ZEC from ZEC_{25} to ZEC_{90}. Ensemble medians of global mean values of ZEC_{25}, ZEC_{90}, and the difference between ZEC_{90} and ZEC_{25} are in parenthesis of titles of (A)–(C) respectively.

shown as a sharp band of warm sea surface temperatures in the Southern and Indian Oceans spanning between longitudes 70° W–175° E in the ZEC_{25} and ZEC_{90} time windows. The continued warming in the Southern Ocean after CO_2 emissions cessation is possibly due to delayed circumpolar upwelling and equatorward transport (Armour *et al* 2016). In terms of continued warming between ZEC_{25} and ZEC_{90} time frames (figure 3(C)), there is negligible warming agreement between the ESMs in the ensemble. Figure S11 in the supplementary material includes mean ZEC distributions, the additional ZEC_{50} time frame, and shows the ensemble spread in ZEC for each time window. There is significant spread of ZEC values regionally with the highest spread located in high latitudes quite possibly due to different model representations related to AMOC and sea-ice coverage (MacDougall *et al* 2022).

Most participating ESMs ran a single ensemble member for the ZECMIP A1 experiment, however two of the nine ESMs ran the experiment with three members (UKESM1-0-LL and CanESM5). As an additional analysis, ZEC regional distributions of the two models with multiple ensemble members were examined to understand how variability within the models compare to mean changes in regional ZEC_{25} and ZEC_{90} patterns. Figures S15 and S19 show regional ZEC projections for each model member ($n = 3$) for CanESM5 and UKESM1-0-LL, respectively. For the CanESM5 data, the three simulations tend to show large land areas with ZEC positive/negative sign agreement during the ZEC_{90} time frame, but less so in the ZEC_{25} time frame. The UKESM1-0-LL members show large areas of ZEC positive/negative sign agreement for both ZEC_{25} and ZEC_{90} time frames. Further investigation is needed to determine more accurate projections of regional ZEC using larger sets of multi-member ensembles than are currently available.

3.2. Local monthly heat extremes

Once 1σ through 3σ local monthly temperature extreme thresholds were computed for each model in the ensemble using methods described in section 2.3, changes in frequencies of local maximum monthly temperature extreme exceedances were computed using the 20 year ZEC_{25} and ZEC_{90} time frames using equations (4) and (5). Figure 4 shows frequencies

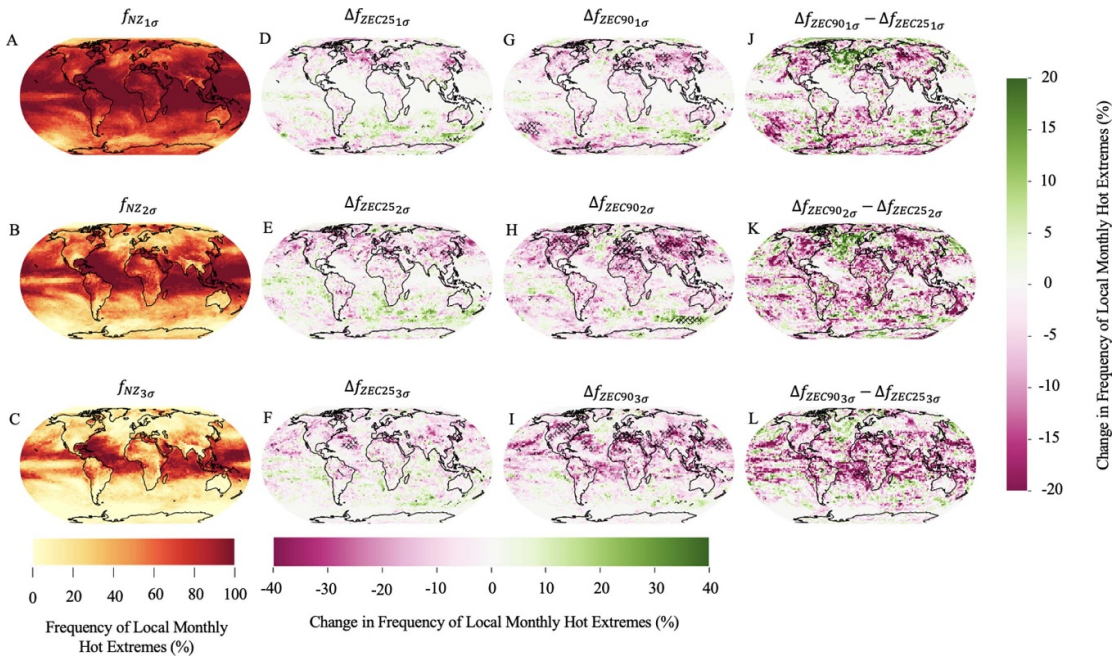

Figure 4. Ensemble median frequency (N years out of 20 expressed as a percentage) of 1σ through 3σ local hot monthly temperature extremes in 20 year net zero baseline climatology (A)–(C). Ensemble median change in frequency (N years out of 20 expressed as a percentage) of 1 σ through 3 σ local hot monthly temperature extremes in ZEC_{25} (DEF) and ZEC_{90} (G)–(I) 20 year time frames. Changes in frequency of local hot monthly temperature extremes for -1σ through 3σ extreme levels, evaluated as the ZEC_{90} frequency distribution subtracted by the ZEC_{25} frequency distribution (J)–(L). Note, the colorbar below the first column correspond to maps (A)–(C), the colorbar below the two middle columns correspond to maps (D)–(I), and the colorbar on the right side of the grid of maps corresponds to maps (J)–(L). Cross-hatching in (D)–(I) indicates that at least 8 models show sign agreement of change in frequency of local hot monthly temperature extremes relative the frequencies from the *1pctCO2* net zero baseline climatology. Cross-hatching in (J)–(L) indicates at least 8 models show sign agreement of change in frequency of local hot monthly extremes over the century after emissions cessation evaluated as ZEC_{90} minus ZEC_{25} frequencies.

of 1σ through 3σ local monthly heat extremes during the net zero baseline climatology, the changes in frequencies of 1σ through 3σ local monthly heat extremes during the ZEC_{25} and ZEC_{90} time frames, and the change in frequency between ZEC_{90} and ZEC_{25} time frames.

During the 20 year net zero baseline time frame, land-based grids exhibit very high frequency of local monthly heat extremes for the 1σ threshold. For 2σ and 3σ thresholds, highest frequencies of local monthly heat extreme exceedances during the net zero baseline climate time frame are largely shown in tropical latitudes due to low variability in the tropics (Hawkins *et al* 2020, Mahlstein *et al* 2011). When the ZEC_{25} time frame is reached, most land surfaces exhibit either no change or a large-scale initial decline in frequency of local monthly heat extreme following CO_2 emissions cessation with some exceptions such as areas of Northern Asia and midwestern North America. In the ZEC_{25} time frame, there are greater decreases in frequencies of land-based monthly heat extremes for 2σ and 3σ thresholds than the decreases in frequencies for the 1σ threshold, especially in tropical latitudes. Although land-based initial reductions in frequency of local monthly heat extremes (especially for 2σ and 3σ thresholds) are evident in many regions, the areas of largest initial decline in frequency of local monthly heat extreme frequency are over land in the Northern Hemisphere. While frequencies of land-based extremes tend to decline during the ZEC_{25} time frame, large oceanic regions have a projected increase in frequency of local monthly heat extremes after CO_2 emissions cessation; specifically, the South Atlantic, Indian Ocean, and Southern Ocean have areas where frequency of local monthly heat extremes are projected to increase with significant model agreement south of Australia. The pattern of increasing oceanic frequencies in the Southern Hemisphere resembles changes in regional ZEC_{25} shown in figure 3(A).

By the ZEC_{90} time frame, there are widespread reductions in frequency of 2σ and 3σ local monthly heat extreme with the largest frequency reductions over land in the Northern Hemisphere. For each extreme threshold, areas of model significance emerge in the ZEC_{90} time frame over land in the Northern Hemisphere. Changes in local monthly heat extreme frequencies during the ZEC_{25} and ZEC_{90} time frames closely follow the mean state regional ZEC_{90} patterns (figure 3(B)) where large-scale land cooling is accompanied by warming in the Southern and Indian Ocean south of Australia.

There are continued reductions in land-based local monthly heat extreme frequencies for the remainder of the century after ZEC_{25} shown in figures 4(J)–(l). These continued reductions in local

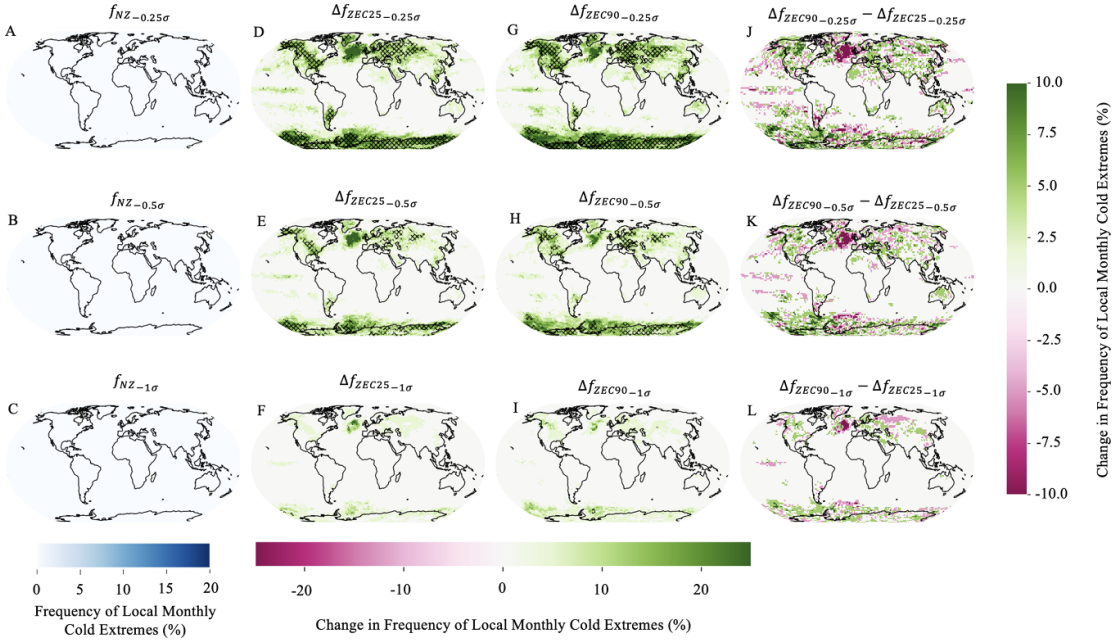

Figure 5. Ensemble median frequency (N years out of 20 expressed as a percentage) of -0.25σ through -1σ local cold monthly temperature extremes in 20 year net zero baseline climatology (A)–(C). Ensemble median change in frequency (N years out of 20 expressed as a percentage) of -0.25σ through -1σ local cold monthly temperature extremes in ZEC_{25} (D)–(F) and ZEC_{90} (G)–(I) 20 year time frames. Changes in frequency of local cold monthly temperature extremes for -0.25σ through -1σ extreme levels, evaluated as the ZEC_{90} frequency distribution subtracted by the ZEC_{25} frequency distribution (J)–(L). Note, the colorbar below the first column correspond to maps (A)–(C), the colorbar below the two middle columns correspond to maps (D)–(I), and the colorbar on the right side of the grid of maps corresponds to maps (J)–(L). Cross-hatching in (D)–(I) indicates that at least 8 models show sign agreement of change in frequency of local cold monthly temperature extremes relative the frequencies from the *1pctCO₂* net zero baseline climatology. Cross-hatching in (J)–(L) indicates at least 8 models show sign agreement of change in frequency of local cold monthly extremes over the century after emissions cessation evaluated as ZEC_{90} minus ZEC_{25} frequencies.

monthly heat extreme frequencies resemble the land response in near-surface air temperature shown in figure 3(C). Despite large land regions showing reductions in heat extreme frequency, there are virtually no areas with significant model agreement. After a small initial decline in frequency of local monthly heat extremes in the northern North Atlantic (especially for 1σ and 2σ), heat extremes in the northern North Atlantic show a rebounding trend after ZEC_{25} time frame shown in figures 4(J)–(l). This northern North Atlantic rebounding trend is also evident in regional ZEC patterns in figure 3 which is possibly due to evolution in AMOC after CO_2 emissions cessation.

Supplementary analysis was done to analyze regional patterns of local monthly heat extreme changes using the two participating ESMs with multiple simulation members (UKESM1-0-LL and CanESM5). Analysis for the two models was performed using identical methods as for the single member analysis discussed in the methods section, and results are found in supplementary information. The results show similar spatial patterns for extreme frequency changes between the three members of each model ensemble, however there are areas where the members show differences in sign changes of local monthly heat extremes; additional members for each ESM would help improve understanding of changes in heat extremes after CO_2 emissions cessation.

3.3. Local monthly cold extremes

Once 0.25σ–1σ local monthly cold temperature extreme thresholds were computed for each model in the ensemble, the change in frequencies of local minimum monthly temperature extreme exceedances were computed using the 20 year ZEC_{25} and ZEC_{90} time frames the same way as above for monthly warm extremes. Figure 5 shows the ensemble median frequencies of local monthly cold extremes, changes in frequencies of local monthly cold extremes after CO_2 emissions cessation, and trends in frequency over the remainder of the century after ZEC_{25} computed as the difference in frequency during ZEC_{90} and ZEC_{25} time frames.

There are virtually no areas where local monthly cold extreme frequencies are elevated during the net zero baseline climatology because of large-scale warming prior to emissions cessation. Note, maps in figure 5 are based on ensemble medians of local cold monthly frequencies, however, there are areas that show slight increases in ensemble *mean* local cold monthly extremes during the net zero baseline climatology as shown in figure S14 of the supplemental material; these areas are clearest over high-latitude grids in the Atlantic Ocean possibly due to reduced

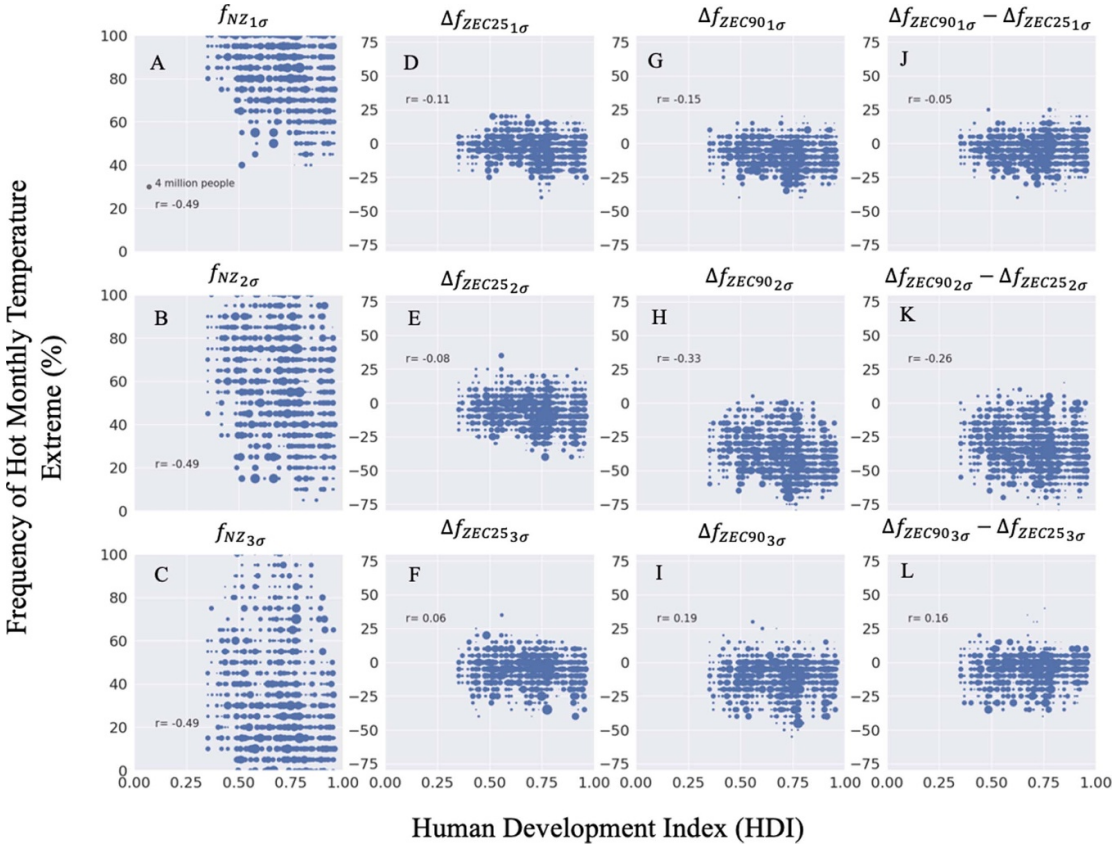

Figure 6. Ensemble median monthly hot temperature extreme frequency in 20 year net zero baseline climatology (A)–(C) plotted against Human Development Index (HDI). Change in ensemble median monthly hot temperature extreme frequency in ZEC_{25} (D)–(F) and ZEC_{90} (G)–(I) windows plotted against Human Development Index. Marker sizes are based on population size, with a reference marker of 4 million people in panel (A). Panels (J)–(L) show the change in local monthly hot temperature extreme frequency evaluated as the ZEC_{90} frequency distribution (G)–(I) subtracted by the ZEC_{25} (D)–(F).

meridional heat transport from weakening AMOC strength during the *1pctCO*$_2$ emissions phase of the experiments.

After CO_2 emission cessation, local monthly cold temperature extremes become more frequent in many extratropical land areas. The most obvious signals are seen in the -0.25σ and -0.5σ thresholds over North America, Europe, Northern Asia, Greenland, southern South America, Australia, and Antarctica. At the -1σ threshold, changes in frequency are very subtle with small frequency increases over Northern Hemisphere land, Antarctica, the northern North Atlantic, and the Southern Ocean; this is because, for all models, global mean temperatures exceed 1 °C warming relative to pre-industrial levels following the *1pctCO2* ramp-up phase of the experiment (see figure S1 in supplementary material). Areas with significant ensemble agreement (eight or more ESMs) of increased local monthly cold extreme frequency are clearest over Northern Hemisphere land, and over Antarctica for -0.25σ and -0.5σ threshold. There are negligible areas with significant ensemble agreement at the -1σ threshold because it is rare to exceed the 1σ threshold at elevated global mean temperature.

Over the remainder of the century after the ZEC_{25}, there are large areas of increasing frequency of local monthly cold extremes, as high as 10%, which are again most evident in the mid-to-high latitudes in North America and northern Asia. There are also regions with reduction in frequency of cold extremes over the remainder of the century after ZEC_{25}; for each σ threshold, the northern North Atlantic ocean exhibits decreased frequency of local monthly cold extremes after the initial increased frequency shown in the ZEC_{25} time frame. Similar to frequencies of local monthly heat extremes, there are very limited areas of significant ensemble agreement (8 or more ESMs) of increasing or decreasing frequency of cold extremes over the remainder of the century after ZEC_{25}.

3.4. Monthly temperature extremes and human development index

Figure 6 shows ensemble median frequency of local hot monthly temperature exceedance during net zero baseline climatology (A)–(C), ensemble median change in frequency of local hot monthly temperature extreme exceedance plotted against HDI for land-based grid cells for the ZEC_{25} (D)–(F), and ZEC_{90} (G)–(I) time frames and the difference between the two time frames (J)–(L).

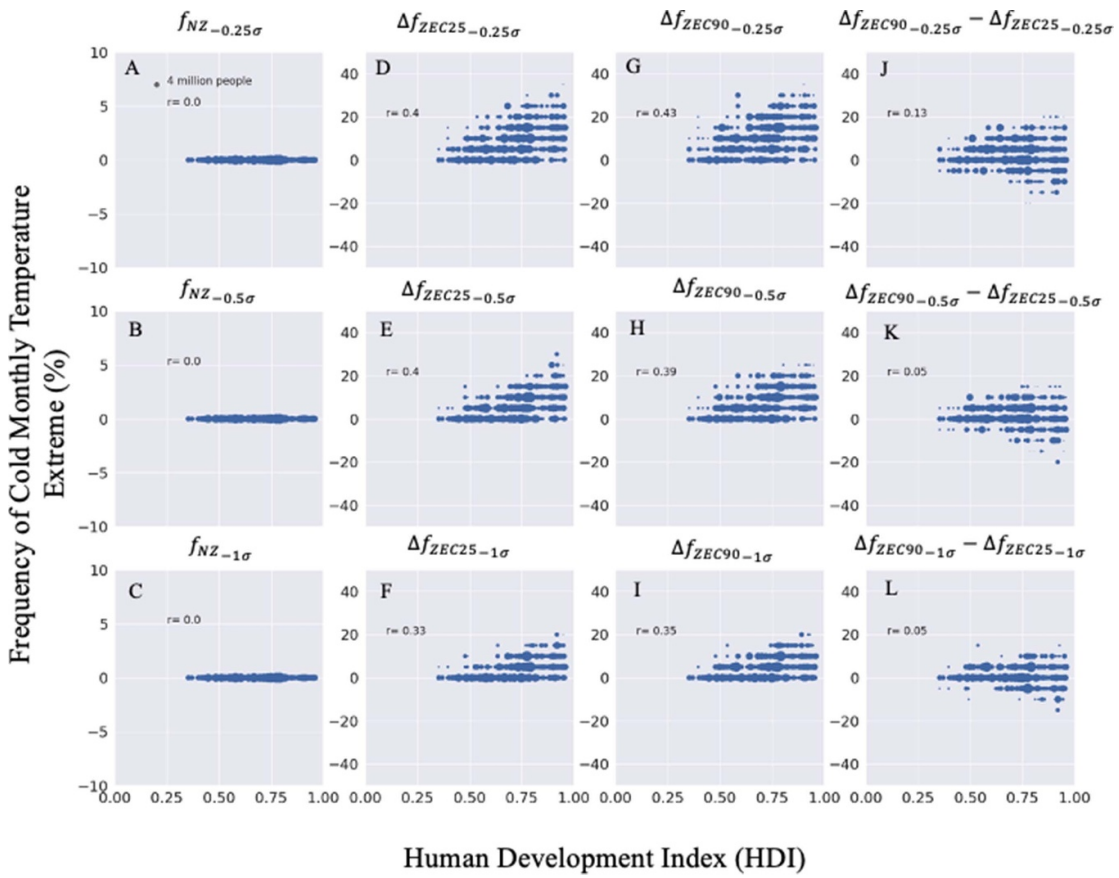

Figure 7. Ensemble median monthly cold temperature extreme frequency in 20 year net zero baseline climatology (A)–(C) plotted against Human Development Index (HDI). Change in ensemble median monthly cold temperature extreme frequency in ZEC_{25} (D)–(F) and ZEC_{90} (G)–(I) windows plotted against Human Development Index. Marker sizes are based on population size, with a reference marker of 4 million people in panel (A). Panels (J)–(L) show the change in local monthly cold temperature extreme frequency evaluated as the ZEC_{90} frequency distribution (G)–(I) subtracted by the ZEC_{25} (D)–(F).

In these results, the Spearman rank correlation is used to understand the overall relationship between changes in local monthly heat extreme frequency and local HDI. The Spearman rank correlation describes statistical dependence between two variables. Spearman rank correlations of -1 or $+1$ indicate that the relationship between two variables is monotonic. As climate change has been shown to disproportionately impact regions of lower socioeconomic development (Harrington *et al* 2016, King and Harrington 2018), a negative Spearman correlation is found (i.e. higher frequencies of heat extremes for lower HDI regions, lower frequency of heat extremes for higher HDI regions). During the 20 year baseline climate, local monthly heat extremes are shown to disproportionately affect lower HDI regions captured by moderately negative Spearman rank correlations in figures 6(A)–(C). During the ZEC_{25} and ZEC_{90} time frames, most land areas experience either no change or reduced frequency of local monthly heat extreme for all σ-levels (shown before in figure 4). Similarly, most grids show either zero change or continued decrease in frequency of local monthly heat extremes shown in figures 6(J)–(L) which is also consistent with results shown in figure 4.

In the ZEC_{25} and ZEC_{90} time frames, 1σ and 2σ distributions have a weakly negative change in Spearman rank correlations which suggests that inequality of climate change remains (and is slightly enhanced) after net zero CO_2. The negative change in Spearman correlations in 1σ and 2σ thresholds are due to larger reductions in frequencies of heat extremes in high HDI mid- to high-latitudes than the reductions in tropical latitudes which tend to have lower HDI, although this is a weak effect and differs slightly from the 3σ results. Over the remainder of the century after the ZEC_{25} time frame, the inequality of climate change for 1σ and 2σ thresholds is slightly enhanced suggested by negative changes in Spearman correlations in figures 6(J) and (K). However, for the 3σ threshold, the inequality of climate change is slightly relaxed based on the positive Spearman correlation in figure 6(l).

In addition to local monthly heat extreme frequency and HDI, we also investigated the relationship between frequency of local monthly cold extremes and HDI. Figure 7 shows the ensemble median change in frequency of local monthly cold temperature extreme exceedance plotted against HDI for land-based grid cells for the 20 year ZEC time frames.

Like figure 6, changes in cold temperature extreme frequency were computed as the difference between ZEC_{90} and ZEC_{25} frequency distributions, and Spearman rank correlations were computed for each distribution.

During the net zero baseline climatology, land-based cold extreme frequencies are negligible based on ensemble median and are supported by results in figures 4(A)–(C). During the ZEC_{25} time frame, increased frequencies in cold extremes are evident across extreme thresholds following CO_2 emissions cessation (figures 7(D)–(F)). Additionally, positive changes in Spearman rank correlations are calculated during the ZEC_{25} time frame due to the emergence in cold extreme frequency over high-HDI Northern Hemisphere land masses as shown in figures 5(D)–(F). The consistently positive Spearman correlations indicate that local cold monthly temperature extremes tend to impact higher HDI regions following CO_2 emissions cessation, which is opposite to heat extreme trends where lower HDI regions continue to experience higher frequency of local monthly heat extremes for 1σ and 2σ thresholds. Over the remainder of the century after the ZEC_{25} time frame, Spearman rank correlations slightly increase which suggests that high HDI land regions will continue to experience higher frequency cold extremes after CO_2 emissions cessation. In terms of ensemble median frequencies of cold extremes, nearly every populated grid cell experiences either no change or an increase in cold extreme frequency similar to the large-scale land-based cooling shown in the mean state regional climate projections post net zero (figure 3).

4. Conclusion

The ESMs included in the ZECMIP 1000 PgC ensemble project large-scale land based cooling during the 100 years following emissions cessation. However, there are significant differences in the value of ZEC regionally, consistent with recently published research (MacDougall *et al* 2022). Land regions are projected to experience a notably cooler local climate compared to the local climate in the 20 year baseline climatology (i.e. the climatology evaluated at the time of branching or emissions cessation). Though most land regions show a consistent cooling response after emissions cessation, there is evidence of continued increase of sea surface temperatures most obvious in the Southern and Indian oceans roughly between longitudes 70° W (Cape Horn, Chile) and 175° E (New Zealand).

Frequencies of local monthly hot temperature extremes are projected to remain either unchanged or decrease following CO_2 emissions cessation. Land-based hot temperature extreme frequencies are projected to decrease as much as 40% within the century after net zero CO_2 emissions, with largest reductions over land in the Northern Hemisphere. Reduction in land-based local monthly temperature extreme frequency within only a century after CO_2 emissions cessation is a promising result, as heat extremes can have severe infrastructural impacts and can lead to loss of life. Within the ZEC_{25} and ZEC_{90} time frames, there are large areas with significant model agreement showing decreasing frequency of local monthly hot temperature extremes, however there are virtually no areas where models show significant agreement of how frequency of high temperature extremes are projected to change over the remainder of the century after ZEC_{25} time frame.

Although frequencies of land-based local monthly heat extremes are projected to remain constant or decrease, results show increasing frequency of extreme exceedance as high as $+20\%$ for $1\sigma-3\sigma$ levels in the North Atlantic, North Pacific, Equatorial Pacific, and the Southern Ocean (especially south of Australia). This contrast between land-based and ocean-based extreme evolution could be an important consideration for planning purposes, as heat extremes can have devastating impacts on marine ecosystems (Garrabou *et al* 2009, Babcock *et al* 2019, Smale *et al* 2019, Holbrook *et al* 2020).

There is evidence of emerging land-based local monthly cold temperature extremes stemming from the rapid cooling over land following emissions cessation, with large scale mid- and high-latitude land regions having the highest increase in frequencies of cold monthly extremes after CO_2 emissions cessation. There is strong model agreement to suggest that the emergence of local monthly cold extremes may be a concern following carbon dioxide emissions cessation, especially for mid- and high-latitude land regions with an emphasis on the Northern Hemisphere. However, like high temperature extremes, there are virtually no areas where changes in frequency of local monthly cold extremes over the century after the ZEC_{25} time frame show significant model agreement.

Over the century after CO_2 emissions cessation, most land areas exhibit a decrease in temperature compared to the ocean due to the relative heat capacities of land and ocean. Decreases in regional temperature after net zero CO_2 are larger over land in mid- and high-latitude Northern Hemisphere compared to tropical and equatorial latitudes. Changes in frequency of local monthly hot temperature extremes follow a similar pattern to regional temperature projections, where tropical and equatorial regions are projected to experience less decrease in local frequency of heat extremes than the decreases projected for mid- to high-latitude Northern Hemisphere. Since tropical and equatorial regions tend to have

lower HDI than mid- to high-latitude Northern Hemisphere regions, the results suggest a continued or slightly enhanced disproportionality of climate change impacts on multi-decadal timescales even after net zero CO_2 emissions are reached.

There is also a relationship between local HDI and changes in monthly cold extreme frequency but it follows the opposite sign as HDI and local monthly heat extremes; increases in the frequency of local monthly cold extremes are largest over the high-HDI Northern Hemisphere where the most significant mean state cooling is projected post-net zero CO_2 emissions. This relationship suggests that cold extremes might impact higher HDI regions, especially mid- and high-latitude Northern Hemisphere, post CO_2 emissions cessation.

This research has focused on idealized simulations of a net zero emissions where models are forced using the *1pctCO$_2$* scenario, which lacks forcing from other greenhouse gases or aerosols, meaning the projections will not represent realistic future trajectories of net radiative forcing at a regional or global scale. In future studies, including other greenhouse gases and aerosols in the experimental setup would be valuable, as scenarios that included short-lived aerosols would likely lead to peak warming within the decade following emissions cessation (Dvorak *et al* 2022). Further investigation of commitments after emissions cessation at multiple cumulative emissions levels is also necessary as climate commitments are expected to change based on cumulative emissions levels at the time of emissions cessation (Ehlert and Zickfeld 2017). The A1 type of experiment used in this study assumes an abrupt transition to zero CO_2 emissions which may introduce an unrealistic jolt to the climate system; future experimental designs might consider smoother transitions to net zero to avoid potential artificial shocks to the climate system in the model projections. In addition, since the ZECMIP ensemble only includes a small sample of models ($n = 9$), additional models would be beneficial for understanding significance and uncertainties and additional members of each model run would help differentiate model results from model internal variability.

Data availability statement

No new data were created or analysed in this study.

Acknowledgments

This work was supported by the Australian Government National Environmental Science Program. The work was also completed with the assistance of resources from the National Computational Infrastructure (NCI), which is supported by the Australian Government.

ORCID iDs

Liam J Cassidy https://orcid.org/0009-0008-2894-6611
Andrew D King https://orcid.org/0000-0001-9006-5745
Josephine R Brown https://orcid.org/0000-0002-1100-7457
Andrew H MacDougall https://orcid.org/0000-0003-1094-6783
Tilo Ziehn https://orcid.org/0000-0001-9873-9775
Seung-Ki Min https://orcid.org/0000-0002-6749-010X
Chris D Jones https://orcid.org/0000-0002-7141-9285

References

Armour K C, Marshall J, Scott J R, Donohoe A and Newsom E R 2016 Southern Ocean warming delayed by circumpolar upwelling and equatorward transport *Nat. Geosci.* **9** 549–54

Babcock R C *et al* 2019 Severe continental-scale impacts of climate change are happening now: extreme climate events impact marine habitat forming communities along 45% of Australia's coast *Front. Mar. Sci.* **6**

Birkmann J *et al* 2022 8 poverty, livelihoods and sustainable development *This chapter should be cited as: Contribution of Working Group II to the Sixth Assessment Report of the Intergovernmental Panel on Climate Change* pp 1171–274

Dai G, Mu M, Li C, Han Z and Wang L 2021 Evaluation of the forecast performance for extreme cold events in East Asia with subseasonal-to-seasonal data sets from ECMWF *J. Geophys. Res. Atmos.* **126**

Dvorak M T, Armour K C, Frierson D M W, Proistosescu C, Baker M B and Smith C J 2022 Estimating the timing of geophysical commitment to 1.5 and 2.0 °C of global warming *Nat. Clim. Change* **12** 547–52

Ehlert D and Zickfeld K 2017 What determines the warming commitment after take back cessation of CO_2 emissions? *Environ. Res. Lett.* **12** 015002

Eyring V, Bony S, Meehl G A, Senior C A, Stevens B, Stouffer R J and Taylor K E 2016 Overview of the coupled model intercomparison project phase 6 (CMIP6) experimental design and organization *Geosci. Model Dev.* **9** 1937–58

Frölicher T L and Joos F 2010 Reversible and irreversible impacts of greenhouse gas emissions in multi-century projections with the NCAR global coupled carbon cycle-climate model *Clim. Dyn.* **35** 1439–59

Gamble J L *et al* 2016 Ch. 9: populations of concern *The Impacts of Climate Change on Human Health in the United States: A Scientific Assessment* (available at: https://health2016.globalchange.gov/downloads#populations-of-concern)

Garrabou J *et al* 2009 Mass mortality in Northwestern Mediterranean rocky benthic communities: effects of the 2003 heat wave *Glob. Change Biol.* **15** 1090–103

Gillett N P, Arora V K, Zickfeld K, Marshall S J and Merryfield W J 2011 Ongoing climate change following a complete cessation of carbon dioxide emissions *Nat. Geosci.* **4** 83–87

Hare B and Meinshausen M 2006 How much warming are we committed to and how much can be avoided? *Clim. Change* **75** 111–49

Harrington L J, Frame D J, Fischer E M, Hawkins E, Joshi M and Jones C D 2016 Poorest countries experience earlier anthropogenic emergence of daily temperature extremes *Environ. Res. Lett.* **11** 055007

Hawkins E, Frame D, Harrington L, Joshi M, King A, Rojas M and Sutton R 2020 Observed emergence of the climate change signal: from the familiar to the unknown *Geophys. Res. Lett.* **47** e2019GL086259

Holbrook N J, Sen Gupta A, Oliver E C J, Hobday A J, Benthuysen J A, Scannell H A, Smale D A and Wernberg T 2020 Keeping pace with marine heatwaves *Nat. Rev. Earth Environ.* **1** 482–93

IPCC 2021 Summary for policymakers *Climate change 2021: the physical science basis Contribution of Working Group I to the Sixth Assessment Report of the Intergovernmental Panel on Climate Change* ed V P Masson-Delmotte *et al* (Cambridge University Press) pp 3–32

Jenkins S, Sanderson B, Peters G, Frölicher T L, Friedlingstein P and Allen M 2022 The multi-decadal response to net zero CO_2 emissions and implications for emissions policy *Geophys. Res. Lett.* **49** e2022GL101047

Jones C D *et al* 2016 C4MIP-the coupled climate-carbon cycle model intercomparison project: experimental protocol for CMIP6 *Geosci. Model Dev.* **9** 2853–80

Jones C D *et al* 2019 The zero emissions commitment model intercomparison project (ZECMIP) contribution to C4MIP: quantifying committed climate changes following zero carbon emissions *Geosci. Model Dev.* **12** 4375–85

Joshi M M, Gregory J M, Webb M J, Sexton D M H and Johns T C 2008 Mechanisms for the land/sea warming contrast exhibited by simulations of climate change *Clim. Dyn.* **30** 455–65

King A D and Harrington L J 2018 The inequality of climate change from 1.5 to 2 °C of global warming *Geophys. Res. Lett.* **45** 5030–3

King A D, Lane T P, Henley B J and Brown J R 2020 Global and regional impacts differ between transient and equilibrium warmer worlds *Nat. Clim. Change* **10** 42–47

Knutti R, Masson D and Gettelman A 2013 Climate model genealogy: generation CMIP5 and how we got there *Geophys. Res. Lett.* **40** 1194–9

Kummu M, Taka M and Guillaume J H A 2018 Gridded global datasets for gross domestic product and Human Development Index over 1990–2015 *Sci. Data* **5** 1–15

Lieber R, King A, Brown J, Ashcroft L, Freund M and McMichael C 2022 ENSO teleconnections more uncertain in regions of lower socioeconomic development *Geophys. Res. Lett.* **49** e2022GL100553

Lowe J A, Huntingford C, Raper S C B, Jones C D, Liddicoat S K and Gohar L K 2009 How difficult is it to recover from dangerous levels of global warming? *Environ. Res. Lett.* **4** 014012

MacDougall A H *et al* 2020 Is there warming in the pipeline? A multi-model analysis of the zero emissions commitment from CO_2 *Biogeosciences* **17** 2987–3016

MacDougall A H, Mallett J, Hohn D and Mengis N 2022 Substantial regional climate change expected following cessation of CO_2 emissions *Environ. Res. Lett.* **17** 114046

Mahlstein I, Knutti R, Solomon S and Portmann R W 2011 Early onset of significant local warming in low latitude countries *Environ. Res. Lett.* **6** 034009

Matthews H D and Caldeira K 2008 Stabilizing climate requires near-zero emissions *Geophys. Res. Lett.* **35**

Matthews H D and Weaver A J 2010 Committed climate warming *Nat. Geosci.* **3** 142–3

Matthews H D and Zickfeld K 2012 Climate response to zeroed emissions of greenhouse gases and aerosols *Nat. Clim. Change* **2** 338–41

Neal E, Huang C S Y and Nakamura N 2022 The 2021 Pacific Northwest heat wave and associated blocking: meteorology and the role of an upstream cyclone as a diabatic source of wave activity *Geophys. Res. Lett.* **49** e2021GL097699

Plattner G-K *et al* 2008 Long-term climate commitments projected with climate-carbon cycle models *J. Clim.* **21** 2721–51

Rugenstein M *et al* 2019 Longrunmip motivation and design for a large collection of millennial-length AOGCM simulations *Bull. Am. Meteorol. Soc.* **100** 2551–69

Sagar A D and Najam A 1998 The human development index: a critical review 1 **25** 249–64

Smale D A *et al* 2019 Marine heatwaves threaten global biodiversity and the provision of ecosystem services *Nat. Clim. Change* **9** 306–12

Zickfeld K *et al* 2013 Long-term climate change commitment and reversibility: an EMIC intercomparison *J. Clim.* **26** 5782–809